Wall Shear Stress Measurements in Two-phase Flow using PIV, an Optical Sensor and Wall Pressure Transducer

E.E. Dominguez-Ontiveros, C.E. Estrada-Perez, Y.A. Hassan

Abstract The effects of microbubbles injected within the boundary layer of a turbulent channel flow were investigated. In this study electrolysis demonstrated to be an effective method to inject microbubbles with an average diameter of 30 μm, and allowed microbubbles to be placed at desired locations within the boundary layer. The wall shear stress in the channel was measured by means of three independent methods: measurement of the pressure gradient by an accurate differential pressure transducer, Particle Image Velocimetry (PIV), and an optical wall shear stress sensor. The three methods showed reasonable agreement of the wall shear stress values for single-phase flow. A decrease in the wall shear stress was noticed with microbubble injection into the boundary layer of the turbulent flow. Complementary information of the microbubble drag reduction phenomenon is obtained when the three independent methods are employed. Skin friction reductions were observed when the microbubbles were injected. Drag reduction of approximately of 10% was observed with small local void fractions.

1
Introduction

Drag reduction in turbulent flow is an important topic for researchers and engineers due to its potential application in several disciplines. The need for energy savings and environmental protection is one of the motives for the recent interest increase in this topic. Energy savings can be a direct result from an adequate control of turbulence. The study of changes of the turbulence properties of a wall-bounded turbulent flow with either a passive or additive apparatus provides knowledge in understanding some of the physical principles that govern turbulence. The ability to forecast, modify and control turbulence has interesting practical applications in the drag reduction field where the most important quantity to be determined is the shear stress.

Many drag reduction investigations have been performed with the injection of polymers and surfactants (Warholic *et al.*, 1999), however less number of documented studies that show drag reduction with injected microbubbles in the boundary layer of channel flows are available in the literature (Madavan *et al.*1985, among others). The presence of pressure gradients and a boundary layer transition on the bluff body introduce difficulties to separate the effects of skin friction and form drag. Therefore, it is necessary to investigate the detailed mechanisms whereby the drag reduction is ocurred.

In 1973 McCormick and Bhattacharyya (1973) reported the first experimental work with the microbubble injection. They used a copper wire wound around a towed body to produce hydrogen bubbles by electrolysis. Migirenko and Evseev (1974) and Bogdevich and Evseev (1976) studied the effects of microbubbles on a turbulent boundary layer using a different injection method. Instead of using electrolysis to generate bubbles, they forced air through a porous surface with pore sizes ranging from 1 to 50 μm. Their experiments were conducted using a simple flat geometry and all measurements were made downstream of the porous section. Drag reductions as high as 80% on flat plate boundary layers have been achieved with the injection of microbubbles (Madavan *et al.*, 1985).

Recently, many researchers have reported drag reduction by injection of gas microbubbles (Guin *et al.*, 1996, Fujikawa *et al*., 2001, Hassan and Ortiz-Villafuerte, 2002 among others). In most of these experiments gas is injected through a porous plate located inside the channel and the measurement of the drag was made by means of different techniques. Fontaine (1999) reported the achievement of more than 80% of drag reduction using a combination of polymers with microbubbles.

E.E. Dominguez-Ontiveros, C.E. Estrada-Perez, Y.A. Hassan

Multiphase Flow Research Laboratory, Department of Nuclear Engineering, Texas A&M University, Texas, USA.
Correspondence to:
Elvis E. Dominguez-Ontiveros, Multiphase Flow Research laboratory, Department of Nuclear Engineering, Texas A&M University, Texas, USA.
E-mail:elvisdom@tamu.edu

In an effort to clarify the mechanism of drag reduction caused by microbubbles, the structure of turbulence in a fully developed channel flow with microbubbles presence has been studied. The study was conducted using the Particle Trackimg Velocimetry technique (PTV) for velocity field measurements. Measurements of pressure gradient using a pressure transducer and wall shear stress quantifications using an optical shear sensor were performed.

Full field of the two-dimensional velocity components within a certain location close to the wall was measured using the PTV technique. Differential pressure fluctuations near the wall zone and punctual shear stress measurements were recorded with an optical sensor. Several records of local void fraction were obtained to study the bubble phase distribution influence on the drag reduction phenomenon. Measurement of the local void fraction distribution within several regions near the channel's wall was performed utilizing the shadowgraphy technique.

2
Experimental set-up

The experiment was carried out in a rectangular cast acrylic channel, whose dimensions are 4.8 m length, 20.6 cm wide and 5.6 cm height. Water was pumped through a closed loop. First water flowed from an elevated tank to the channel by gravity. Then, water was conducted to a storage tank; from which water was pumped back to the elevated tank. The upper tank has a constant water head maintained by the pumps. A schematic diagram of the experimental set up is illustrated in Figure 1 and a photograph of the components is shown in Figure 2.
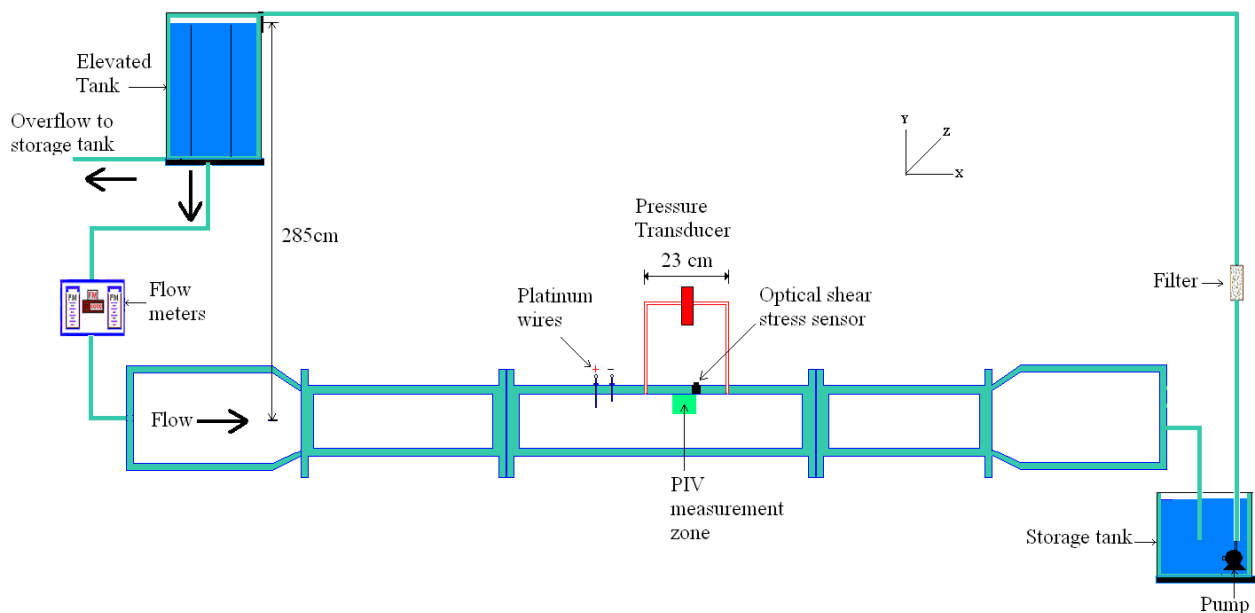

Figure 1. Schematic experimental set-up.

The velocity field in the X-Y plane is obtained by particle tracking velocimetry at 3.15 m downstream the channel inlet (length-to-hydraulic-diameter-ratio= 36). An Nd:YAG laser with a wavelength of 532 nm (green light) and power of 350 mJ per pulse is utilized in the viewing area zone. The particle seeds used for tracing the flow have small diameters range from 6 to 9 μm with specific gravity of 1.01 close to water's specific gravity.

The scattered laser light from the seeding particles was recorded using a CCD Kodak Megaplus camera, Model ES 1.0, 1008 x 1018 pixels. The viewing area was 1.28 cm^2 and was located close to the upper channel's wall. The system recorded 30 velocity fields per second. Each velocity field was obtained from a pair of consecutive images capturing the second image of the pair 1ms after the first one via frame straddling approach. Images were recorded for a time span of approximately 3.3 sec.

The pressure gradient in the test section was measured with pressure taps positioned on the top wall of the channel over a distance of 23 cm. A Validyne pressure transducer (Model DP103) was used. This device utilizes a central diaphragm as a sensor element and is of the variable reluctance type. Because the diaphragm needs to move only one or two thousandths of an inch to produce a full scale output, the thickness and area of the diaphragm

determines the full-scale pressure range. A large diaphragm made of thin foil will respond to extremely low pressures. Conversely, a thick diaphragm with a small area responds to very high pressures. The transducer has a range of pressure difference of 0 to 35 ± 0.09 Pascal. To obtain the wall shear stress from the pressure drop measurements for fully two dimensional single-phase channel flows, the following equation can be utilized:

$$\tau_w = -H \frac{\Delta P}{\Delta x}$$ (1)

where, τ_w is the wall shear stress, ΔP is the pressure drop measured by the pressure transducer, Δx is the axial distance between the pressure connection tabs and H is the half width of the channel.
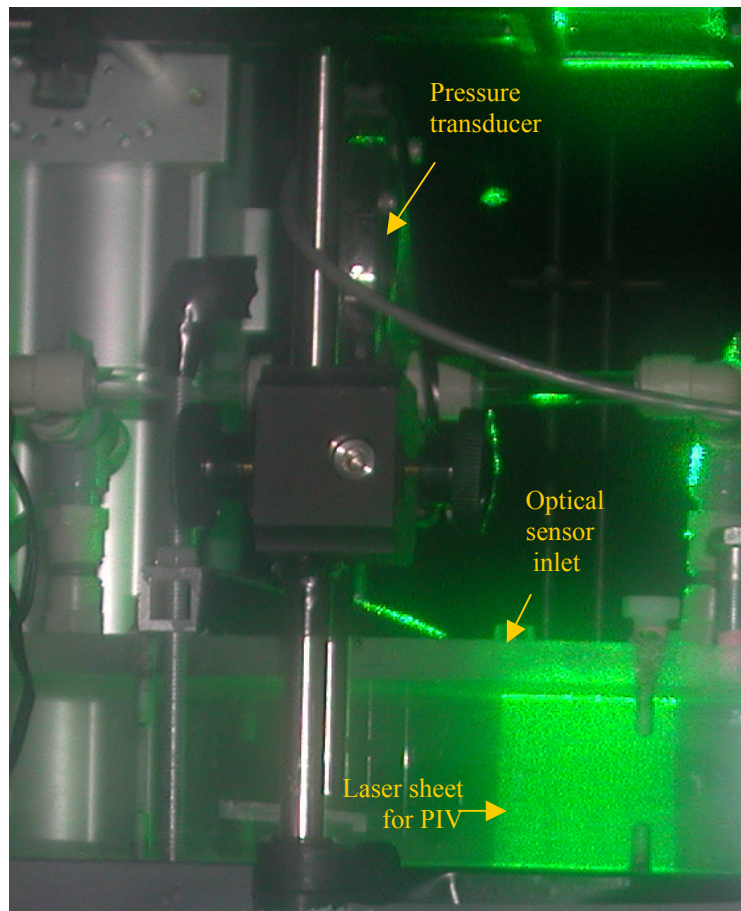

Figure 2. Photograph of the components.

An optical shear stress sensor was also used in the present study to measure wall shear stress fluctuations. The sensor's principle of operation is based on a measurement technique using the Divergence Fringe Doppler theory. Its principle is very similar to the well-known Laser Doppler Velocimetry (LDV). A laser beam is passed through an array of optical elements to obtain a divergent interference fringe pattern originated at the surface of the sensor and extending into the flow (Gharib et al., 2001). The scattered light from the particle passing through the fringes is collected through a window at the surface of the sensor and focused onto a multimode fiber by the receiver diffractive optical element.

The probe volume region is defined by the intersection of the transmitter and receiver fields centered at approximately 66 μm above the surface (see Figure 3). Detailed information about the sensor specific characteristics is given by Fourguette (2003). The optical shear stress sensor system includes a low pass filter, which limits the frequency output of the burst produced by the particles crossing the Doppler fringes. One of the differences between the Laser Doppler Velocimetry and the optical shear stress sensor is that LDV uses a set of parallel fringes at the

probe volume to measure the velocity, while the shear stress sensor uses a set of diverging fringes to measure the gradient of the velocity.

The local fringe separation, δ, is prestablished by the fabricant and is linear to the distance from the sensor, y. Using k as the fringe diverging rate, the velocity of a particle crossing the measurement volume is obtained from:

$$u = f \times \delta \tag{2}$$

The Doppler frequency, f, multiplied by the fringe divergence rate yields the velocity gradient in the quasi-linear sublayer of the boundary layer.

$$\frac{u}{y} = f \times k \tag{3}$$

These expressions basically mean that the sensor measures the velocity at a distance of 66 μm from the micro optical elements. Then these measurements are used to obtain the velocity gradient since the divergence rate of the fringes is known. Finally, the wall shear stress is obtained by multiplying the frequency (in Hz) times the water viscosity, μ.
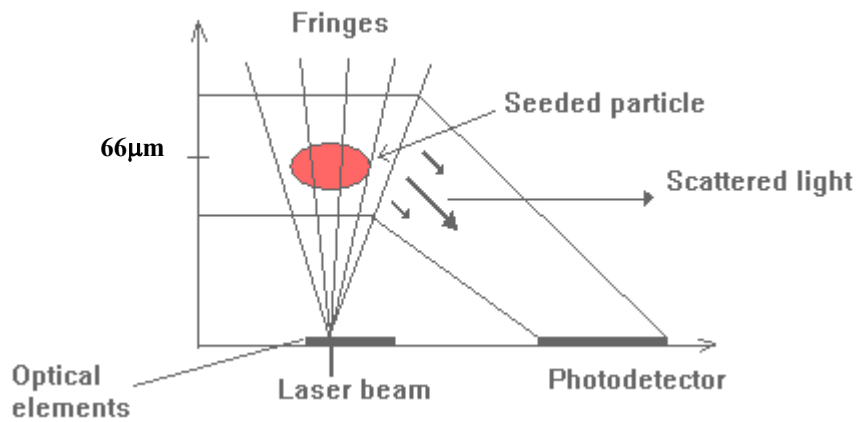

Figure 3. Optical shear stress sensor elements.

The hydrogen microbubbles used to achieve drag reduction are produced by electrolysis located at 10 cm upstream the test zone. Platinum wires with a diameter of 76 μm are used as electrodes, as shown in Figure 4. This figure presents the lateral and top views of the microbubble regime. It also delineates the microbubble sheet dispersion. To produce hydrogen microbubbles of 30 μm, a current of 25 mA is conducted through the electrodes. The negative electrode (cathode) produces hydrogen microbubbles whereas the positive one (anode) produces oxygen microbubbles.

3
Results and discussion

The tests were carried out with various volumetric water flow rates to achieve various Reynolds numbers. The Reynolds number (Re_h) is calculated using the half height of the channel, the bulk velocity and the viscosity of water. The following section presents the results for $Re_h \cong 5128$. Two-phase flow measurements with various void fraction values were obtained. The average bubble size was 30 μm. The void fraction value within the measurement zone was estimated using the following relation:

$$\alpha = \frac{V_g}{V_g + V_l} \qquad (4)$$

where V_g is the volume of the gas bubbles in the viewing volume with thickness of about 1 mm and V_l is volume of the liquid water in the viewing volume.
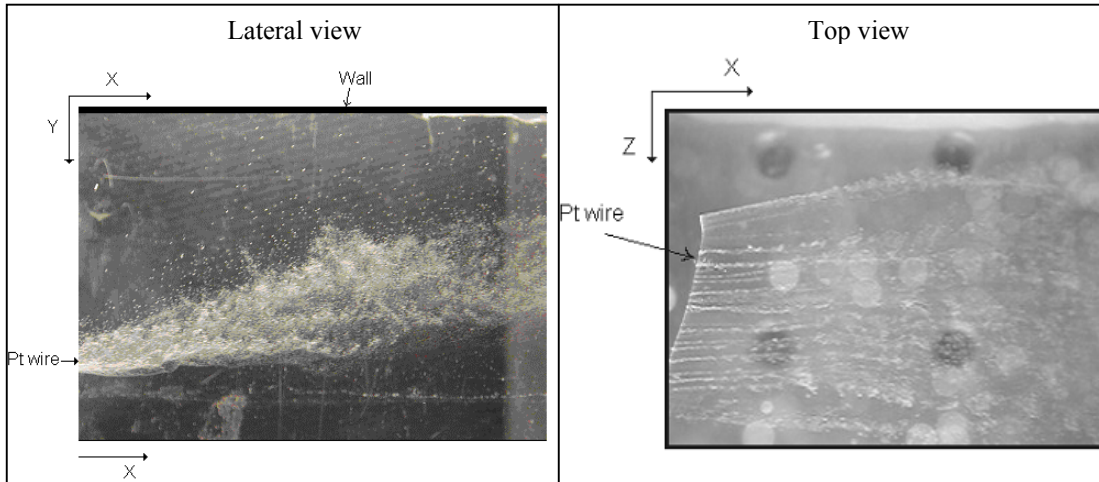

Figure 4. Microbubbles injection.

In this study, the particle tracking routine is a cross correlation algorithm. Two different software applications were used for the tracking process. The resulting velocity vectors from each application were then compared and combined. This hybrid tracking technique greatly increased the total number of velocity vectors used for the flow field analysis. The first software allows online image processing and tracking of the particle tracers (Uemura *et al.* 1991). Thus, the image threshold and tracking parameters can be correctly set for a whole data set. This program is considered robust and reliable in particle centroid determination and tracking. The other tracking program and particle centroid determination algorithm are home-developed routines (Hassan *et al.* 1992), and these routines have been improved over the years.

3.1 PIV Analysis
Once the velocity vectors were obtained from both particle-tracking algorithms, they undergo a filtering process. Statistical filters were applied independently to the vector data sets from each tracking process. The first filter was the cross correlation value itself. In our case, only those vectors with a cross correlation coefficient value higher than the average value, sometimes minus a standard deviation, of a whole vector data set were considered for the flow field analysis. Some of the rejected vectors can easily be seen as erroneous vectors. They are vectors with direction and/or magnitude far deviated from the neighbors. The second filter function, removed vectors that were not within the average plus or minus a standard deviation value from the magnitude and direction of the representative velocity vector in a small window. This step ensures that velocity gradients were correctly delineated. In this step about 10% of the vectors were removed. Finally, the remaining vectors from each process were analyzed separately to obtain instantaneous velocity fields. Besides, space and time averaged velocity fields were calculated in order to obtain statistical parameters of the flow. A typical time-averaged velocity field is shown in Figure 5. The contour color plot elucidates the magnitude of velocity gradients present at the boundary layer.

The average number of instantaneous velocity vectors within the viewing area of approximately $1cm^2$ was about 1500. Instantaneous velocity vector fields were interpolated applying the inverse distance algorithm using windows of 20x20 pixels. As a result of the interpolation process, the final instantaneous velocity fields have a vector distribution of 50x50 vectors. Once the vectors are distributed in the regular interpolation mesh (50x50) the viscous component of the total shear stress can be determined from the measured streamwise velocity profile. The derivative dU/dy was calculated using the central difference scheme.
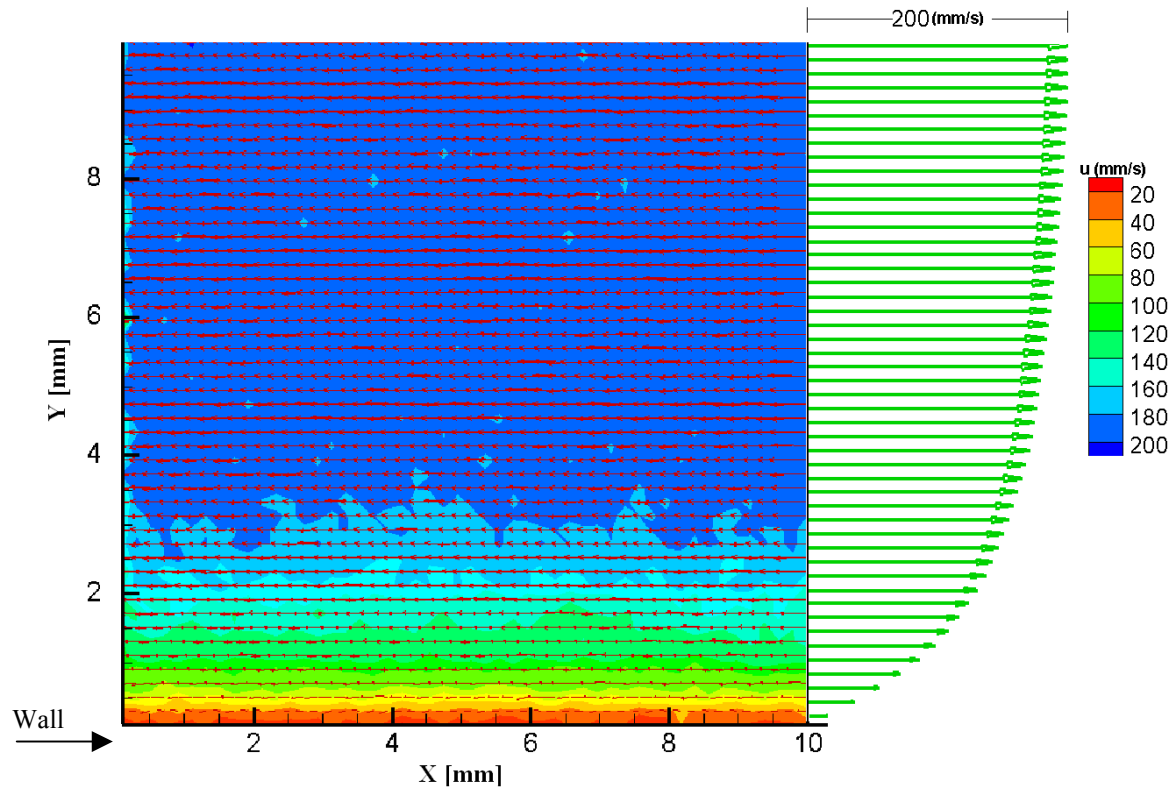
Figure 5. Typical time-averaged velocity field and its correspondent velocity profile, Re=5128.

The conditions of the various void fraction test cases for Re of 5128 are summarized in Table 1. These results confirm that drag reduction has a strong dependence on the local void fraction values. The average bubbles diameter, d^+ is presented in wall units which friction velocity u_τ, is calculated from equation (5).

The non-dimensional d^+ is computed from equation (6). Comparison between the length-scales present within the boundary layer and the non-dimensional bubble's size is important from the physical mechanism point of view in this regime.

$$u_\tau = \sqrt{\frac{\tau_w}{\rho}}$$ (5)

$$d^+ = \frac{d u_\tau \rho}{\mu}$$ (6)

Experiment	Uτ (m/s)	d⁺	Void Fraction (α)	Drag Reduction
Single-phase	0.0116	-	-	-
Case 1	0.0108	0.32	2.40%	12%
Case 2	0.0106	0.31	3.40%	16%
Case 3	0.0097	0.29	4.40%	28%
Case 4	0.0091	0.27	4.90%	38%

Table 1. Summary of two-phase flow cases studied.

3.2 Optical Sensor

Figure 6 shows typical burst outputs obtained form the optical shear stress sensor for the single-phase flow and the case with microbubble injection. The *X*-axis shows the non-dimensional time and the *Y*-axis shows voltage. It can bee seen that the shape of the output is similar for both cases but the burst's amplitude change. Irregularities at the beginning and the end of the output burst can be noticed for the case when the microbubbles are injected. Light scattering of the microbubbles causes these irregularities. It is of considerable concern to distinguish between bubbles and the seeded particles in the flow. Since microbubbles and particles can cross the measurement volume of the shear stress sensor, the analysis of the result was based on the different effect of the microbubbles and seeds. This effect was obtained based on the fact that microbubbles and the seeded particles have a different refractive index. Comparison of the amplitude of the output burst from the shear stress sensor when only the seeded particles are present in the flow against the burst amplitude with only microbubbles presence in the flow yields a characterization of the output bursts.

The importance of removing the burst generated by the microbubbles relies on the fact that, the need is to determine the velocity of the fluid phase and not the velocity of the gas phase. Once the bursts have been obtained for the different data sets, a power spectrum algorithm based in the application of the Fast Fourier Transform, was used to extract the characteristic frequency of each burst. This frequency determines the velocity in Hz, for the particles crossing the Doppler fringes within the measurement volume.
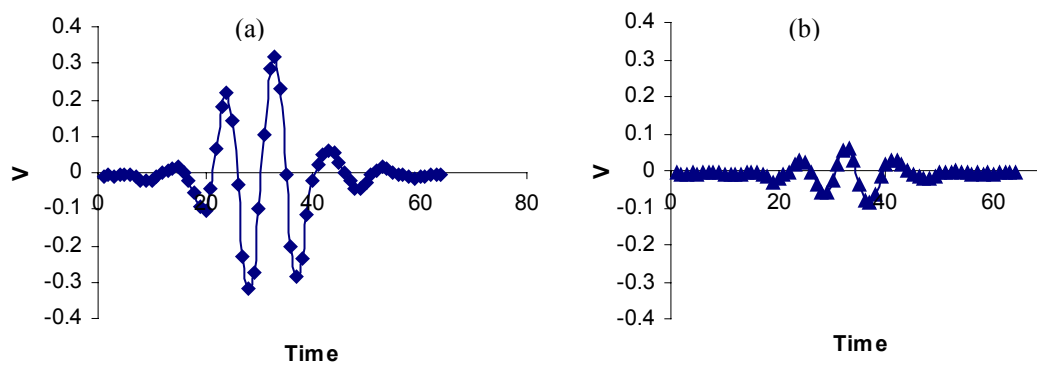
Figure 6. Typical burst output from the diverge fringe Doppler sensor (after filtration) for a) single-phase flow b) Two phase flow.

Table 2 summarizes the results obtained from the shear stress sensor. There was a reduction in the wall shear stress when the microbubbles were injected. Table 3 presents the wall shear stress measured in Pascal. These results were obtained with a local void fraction of 2.4% since the sensor decrease considerably its performance when higher local void fractions were present at the measurement zone. The cause for this decrease is the eventual attachment of some microbubbles to the top channel wall, which in turn changes the measuring conditions explained before for optimal performance of the sensor.

Re=5128	Mean (Hz)	Median (Hz)	Mode(Hz)	$\sqrt{\overline{u'^2}}$ (Hz)
Single-phase	2269	2258	2274	480
Two-phase	2040	1994	2116	396

Table 2. Statistical results from the optical shear stress sensor.

Re=5128	τw (Pa)	Drag Reduction
Single-phase	0.15	
Two-phase	0.135	10%

Table 3. Average wall shear stress measured with the optical sensor.

3.3 Pressure Transducer

The measured value of pressure drop can be transformed to its correspondent value of wall shear stress using equation (1). The continuous pressure signal was sampled at a frequency rate of 1000 Hz to obtain a discrete representation of the differential pressure fluctuations. Figure 7 shows a typical output of the discretized pressure signal for single phase and two phase flow. The X-axis represents the wall shear stress calculated using the pressure drop in Pascals (Pa), and the Y-axis represents the acquisition time. Once again, the pressure signal shows a decrease in the wall shear stress when the microbubbles were injected within the boundary layer of the channel flow. The nature of the pressure fluctuations indicate changes in the wall pressure that in turn, could be related to the turbulence structures in the fluid.
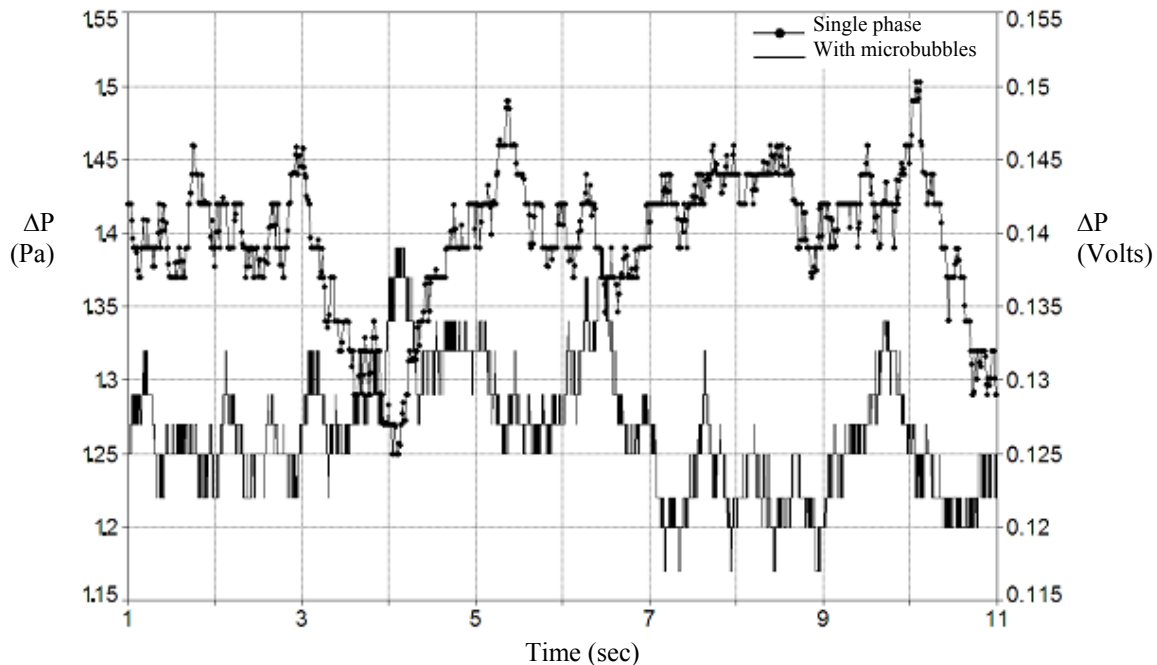
Figure 7. Differential pressure vs Time, Re=5128, original pressure signal for single and two-phase flow.

Table 4 presents the average wall shear stress values obtained with a local void fraction of 2.4%.

Re=5128	τw (Pa)	Drag Reduction
Single-phase	0.16	
Two-phase	0.144	10%

Table 4. Average wall shear stress calculated from the wall pressure drop.

Table 5 shows the results of the wall shear stress using the three methods for single-phase flow and with microbubble injection for a local void fraction, $\alpha=2.4\%$.

Re=5128 α=2.4%	Method		
	PIV	Optical Sensor	Pressure Drop
	$\tau_w = -\mu\dfrac{\partial u}{\partial y}$	$\tau_w = -\mu(f \times k)$	$\tau_w = -H\dfrac{\partial P}{\partial x}$
	(Pa)	(Pa)	(Pa)
Single-Phase	0.15	0.15	0.16
Two-Phase	0.13	0.13	0.14

Table 5. Comparison of the obtained wall shear stress by the three methods.

4
Conclusions

In this study, the three methods proposed for quantification of drag-reduction shown to be in good agreement (see Table 5). All of them showed a decrease in the wall shear stress when the microbubbles were injected into the boundary layer of the turbulent flow. An average drag reduction of 10% was observed for local void fractions of 2.4% by the three methods. The Particle Tracking Velocimetry technique elucidates a higher drag reduction of as much as 38% for a local void fraction of 4.9%. The methods used to measure the wall shear stress offer complementary information for the understanding of the drag reduction phenomena. However, each method has its own advantages and disadvantages.

The PTV system used in this study has the advantage of an acceptable spatial resolution but poor temporal resolution. In addition, the PTV technique performed satisfactory for the various void fractions studied. The optical shear stress sensor has the advantage of great time resolution but a poor spatial resolution. The frequency response of this system reaches the MHz range although its spatial resolution is limited since it measures the wall shear stress at a specific location. The optical sensor proves to be in good agreement with the expected values of wall shear stress for single-phase flow. However, the optical sensor shows operational limitations at high local void fractions.

Finally, the wall pressure measurements method has the advantage of a good sensitivity but a poor time resolution. The wall-pressure gradient measurements proved to be a reasonable tool for the measurement of drag reduction. As opposed to the PIV and the optical sensor, this method does not require the flow to be seeded with external particles. Values of the instantaneous wall shear stress can be obtained by direct observation of the pressure signal, which could help in the design of systems capable of controlling the skin friction based on a feedback given by the wall-pressure signal.

References

Bogdevich V G; Evseev A R (1976) Effect of gas saturation on wall turbulence, in investigations of boundary layer control. Eds. S.S.Kutateladze and G.S. Migirneko, Thermophysics Institute Publishing House, p.49.

Fontaine A A; Deutsch S; Brungart T A; Petrie H L; Fenstermacker,M (1999) Drag reduction by coupled systems: Microbubble injection with homogeneous polymer and surfactant solutions. Experiments in Fluids, **26**, 397-403.

Fourguette D; Modarress D; Wilson D; Koochesfahani M; Gharib M (2003) An optical mems-based shear stress sensor for high Reynolds number applications. Private communication VioSense Corporation. Pasadena, CA. Available at http://www.viosense.com/publications.shtmlT

Fujikawa S; Zhang R; Hayama S; Peng G (2001) The control of micro air-bubble generation by a rotational porous plate. In Proceedings of the 4th International Conference on Multiphase Flow '01, New Orleans,LA,USA,171-179, ICMF01.

Guin M M; Kato H; Yamaguchi H; Maeda M; Miyinaga M (1996) Reduction of skin friction by microbubbles and its relation with near wall concentration in a channel. Journal of Marine Science and Technology, **1**, 246-254.

Gharib M; Modarness D; Fourguette D; Wilson D (2001) Optical microsensor for fluid flow diagnostics. American Institute of Aeronautics and Astronautics, Inc.

Hassan Y A; Blanchat T K; Seeley Jr C H; Canaan R E (1992) Simultaneous velocity measurements of both components of a two-phase flow using particle image velocimetry. Int J Multiphase Flow, **18**, 371-395.

Hassan Y A; Ortiz-Villafuerte J (2002) Experimental study of micro-bubble drag reduction using particle image velocimetry. In 11th International Symposium on Applications of Laser Techniques to Fluid Mechanics. Lisbon, Portugal, **23**, 2.

Madavan N K; Merkle C L; Deutsch S (1985) Numerical investigations into the mechanisms of microbubble drag reduction. Journal of Fluids Engineering, **107**, 370-377.

McCormick M E; Bhattacharyva R (1973) Drag reduction of a submersible hull by electrolysis. Naval Engineers Journal, 11-16.

Migirenko G S; Evsev A R (1974) Turbulent boundary layer with gas saturation, in Problems of thermophysics ans physical hydrodynamics, Novorsivisky Mauka.

Uemura T; Yamamoto F; Ohmi K (1991) Mixing flow in a cylindrical vessel agitated by a bubbling jet. Application of Laser Techniques to Fluid Mechanics. Springer-Verlag, 512-536.

Warholic M D; Massah H; Hanratty T J (1999) Influence of drag reducing polymers on turbulence: Effect of Reynolds number, concentration and mixture. Experiments in Fluids, **27**, 461-472.